Cyclic peptide-poly(HPMA) nanotubes as drug delivery vectors: *in vitro* assessment, pharmacokinetics and biodistribution.

Sophie C. Larnaudie,[a,b] *Joaquin Sanchis,*[b] *Tri-Hung Nguyen,*[b] *Raoul Peltier,*[a] *Sylvain Catrouillet,*[a] *Johannes C. Brendel,* ǂ [a,b] *Christopher J. H. Porter,*[b,c] *Katrina A. Jolliffe,*[d] *and Sébastien Perrier**[a,b]

[a] Department of Chemistry, University of Warwick, Gibbet Hill Road, Coventry CV4 7AL, United Kingdom.

[b] Drug Delivery, Disposition and Dynamics, Monash Institute of Pharmaceutical Sciences, Monash University, 381 Royal Parade, Parkville, VIC 3052, Australia.

[c] ARC Centre of Excellence in Convergent Bio-Nano Science and Technology, Monash Institute of Pharmaceutical Sciences, Monash University, Parkville, VIC 3052, Australia

[d] The University of Sydney, School of Chemistry, Building F11, Sydney NSW 2006, Australia.

ǂ Current address: Jena Center for Soft Matter (JCSM), Friedrich-Schiller-University, Philosophenweg 7, 7743 Jena, Germany.

*s.perrier@warwick.ac.uk

Abstract

Size and shape have progressively appeared as some of the key factors influencing the properties of nanosized drug delivery systems. In particular, elongated materials are thought to interact differently with cells and therefore may allow alterations of *in vivo* fate without changes in chemical composition. A challenge, however, remains the creation of stable self-assembled materials with anisotropic shape for delivery applications that still feature the ability to disassemble, avoiding organ accumulation and facilitating clearance from the system. In this context, we report on self-assembled cyclic peptide-polymer conjugates that self-assemble into supramolecular nanotubes, as confirmed by SANS and SLS. Their behaviour *ex* and *in vivo* was studied: the nanostructures are non-toxic up to a concentration of 0.5 $g.L^{-1}$ and cell uptake studies revealed that the pathway of entry was energy-dependent. Pharmacokinetic studies following intravenous injection of the peptide-polymer conjugate and the control polymer to rats showed that the larger size of the nanotubes formed by the conjugate reduced renal clearance and elongated systemic circulation. Importantly, the ability to slowly disassemble into small units allowed effective clearance of the conjugates and reduced organ accumulation, making these materials interesting candidates in the search for effective drug carriers.

Keywords

Peptide-polymer conjugates, supramolecular nanotubes, radiolabelling, pharmacokinetics, biodistribution.

Introduction

Nanomedicine, and the use of drug delivery systems in particular, has been shown to reduce drug related side effects and thus to allow for higher drug dosing.[1-2] Nanosized carriers with

stealth like surface permits enhanced circulation times by avoiding immediate renal filtration and unspecific organ accumulation, which can enable passive targeting to tumors by the enhanced permeability and retention (EPR) effect.[3-4] Delivery vectors also provide shielding of the drug,[5] and allow for the introduction of targeting moieties,[6-8] thus reducing side effects and enhancing drug delivery efficiency. Amultitude of drug delivery vectors have been explored in the past decades with variable degree of success, including inorganic (gold nanoparticles,[9] quantum dots,[10] silica nanoparticles[11]) and organic (lipid formulations,[12-13] viral nanoparticles,[14] carbon nanotubes[15] or polymer-based structures[16]) carriers.

Shape has progressively appeared as one of the features that may influence the *in vivo* behaviour of carriers, with elongated structures attracting increasing attention.[17] Some studies have shown that because of their increased aspect ratio, elongated nanoparticles exhibit longer circulation times and can enhance tumour accumulation *in vivo*.[18] Filomicelles,[19] polymer brushes[20] and PEGylated tobacco mosaic viruses[21-22] are among organic tubular structures that have shown promising results *in vivo.* Discher *et al.* have, for example, studied filomicelles and compared their behaviour to that of their spherical counterparts in mice models.[23] They showed that large cylindrical structures of 2-18 µm in length enable much longer circulation times and higher loading of the anticancer agent Paclitaxel in comparison to spherical particles while maintaining similar tumour accumulation and survival rates. Müllner *et al.* have studied the pharmacokinetics of unimolecular cylindrical polymer brushes (with lengths ranking from 35 nm to 1200 nm) in rats, showing that they exhibit long term blood circulation, and that the aspect ratio of the brushes has a considerable impact on their pharmacokinetic parameters.[24] They further studied this system in mouse xenografts, demonstrating that the brushes undergo EPR and passively target tumour tissues.[25] The main limitation of such large stable objects is their high stability in vivo leading to relatively poor clearance, which may lead to recognition

by the mononuclear phagocytic system (MPS) translating to high accumulation in organs such as the spleen and the liver.[26]

One way to circumvent this issue is to explore the use of materials which undergo supramolecular self-assembly, for example by directed hydrogen bonds formation.[27-29] Supramolecular polymers,[30] especially those that self-assemble in aqueous media,[31] have started to gain considerable attention in the field of nanomedicine.[27] They allow for a bottom-up design strategy that enables extensive functionalization of the building blocks, resulting in broad libraries of assembled materials. Examples include systems based on host-guest interactions,[32] or on the stacking of peptide amphiphiles into fibres.[33-35] One possible major advantage of self-assembling structures over other nanoparticles is their supramolecular nature which provides initial stability, but eventually allows the structures to break up into unimeric entities small enough to be cleared out of the system, hence avoiding undesired organ accumulation.

An emerging class of elongated drug carriers that feature such a supramolecular structure are nanotubes comprising cyclic peptide-polymer conjugates.[36] Cyclic peptides formed of an even number of alternating D- and L- amino acids have been shown to adopt a flat conformation leading to stacking into nanotubes through antiparallel β-sheet formation.[37] Conjugation of water-soluble polymers to these peptides enables control over the size and the functionality of the nanotubes. Although first cell studies indicated that nanotubes possess great potential as nanosized drug delivery systems,[38-40] their *in vivo* behaviour has yet to be explored.

Here, we synthesized poly(hydroxypropyl methacrylamide) (pHPMA)-based cyclic-peptide polymer conjugates and examined their ability to self-assemble into nanotubes. A non-assembling polymer which does not contain the peptide core was also synthesised as a control. After selection of the most promising candidate, the *in vitro* behaviour of both conjugate and

control polymer, as well as their pharmacokinetics and biodistribution in rats were studied and compared.

Results and discussion

Design and synthesis

The choice of a polymer that is pharmaceutically relevant is critical when designing a drug delivery vector, which is why pHPMA was chosen. During the past decades, pHPMA has been extensively studied in the context of cancer therapy[41] and several polymer-drug conjugates based on this polymer are in different stages of clinical trials.[42-43] In addition to its high biocompatibility, pHPMA can be accessed by radical polymerization methods, which facilitates the introduction of comonomers and the formation of defined end-groups. Three pHPMA-cyclic peptide conjugates were synthesized, using Reversible Addition Fragmentation Chain Transfer (RAFT) polymerization (see details in materials and methods section and supporting information) followed by coupling of the polymer to the chosen cyclic peptide, cyclo(D-Leu-Lys-D-Leu-Trp)$_2$ (Scheme 1 and

Table 1). Two different degrees of polymerization (DP) were targeted for HPMA homopolymers (**P1**, DP = 25 and **P2**, DP = 50). A third polymer (**P3**, DP = 50) incorporating a small percentage of a pyridine-containing comonomer (PUEMA), which provides a handle for attachment of organometallic drugs, was also prepared to test the influence of functional handles introduction in the system.

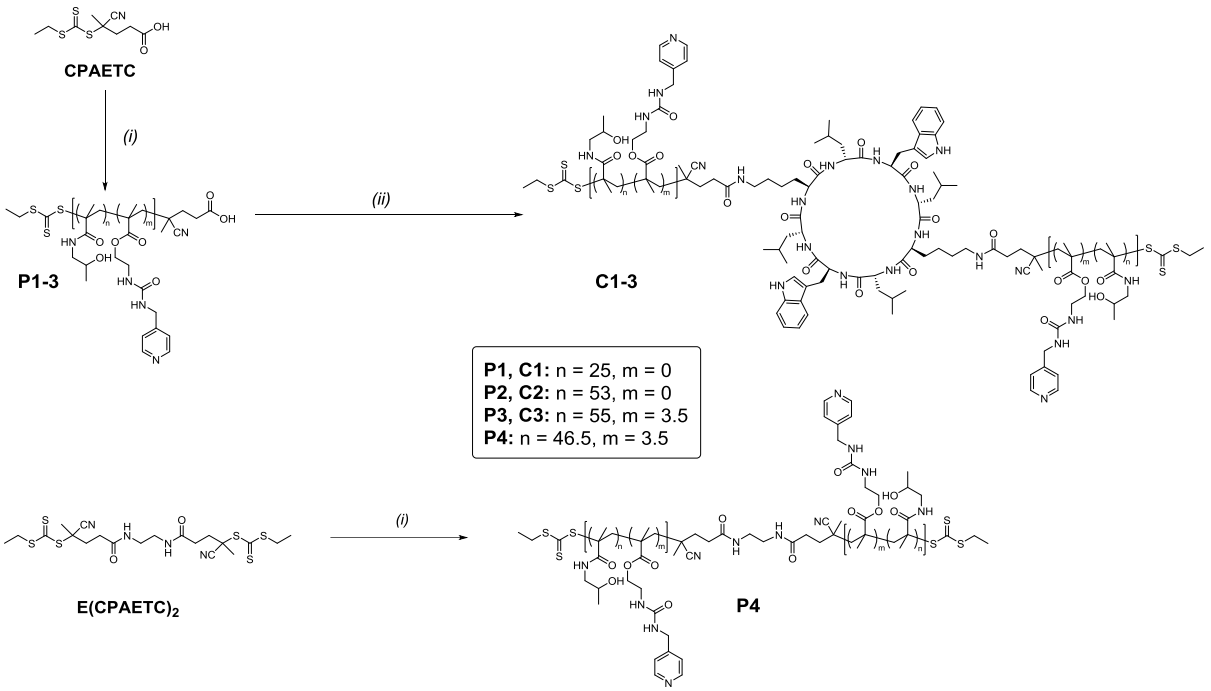

Scheme 1. Synthesis of polymers **P1-4** and conjugates **C1-3**. (*i*) HPMA, VA 044, DMSO/H_2O (opt: 5% PUEMA). (*ii*) cyclo(D-Leu-Lys-D-Leu-Trp)$_2$, HBTU, NMM, DMSO.

As expected from RAFT polymerization, all obtained polymers **P1-3** displayed low dispersities ≤ 1.15. The polymers were subsequently attached to cyclo(D-Leu-Lys-D-Leu-Trp)$_2$, *via* amide bond formation between the carboxylic acid chain end of the polymers and the two lysine residues present on the cyclic peptide, using *O*-(benzotriazol-1-yl)-*N,N,N′,N′*-tetramethyluronium hexafluorophosphate (HBTU) as a coupling reagent in the presence of an organic base, to form a stable amide bond.[44-46] The obtained peptide-polymer conjugates **C1-3** were purified by dialysis and isolated. Size exclusion chromatography (SEC) analysis revealed that low dispersities (≤ 1.20) were maintained (see Figure S1 for SEC chromatograms).

Table 1. **Summary of polymers and conjugates used in this work.**

Entry	**Material**	$M_{n,\,th}$[a] (g.mol^{-1})	$M_{n,\,GPC}$[b] (g.mol^{-1})	$Đ$[b]

P1	$pHPMA_{25}$	3900	7000	1.10
C1	$CP\text{-}(pHPMA_{25})_2$	8800	14200	1.13
P2	$pHPMA_{53}$	7800	11700	1.10
C2	$CP\text{-}(pHPMA_{53})_2$	16600	27900	1.12
P3	$p(HPMA_{55}\text{-}co\text{-}PUEMA_{3.5})$	9100	11900	1.10
C3	$CP\text{-}(p(HPMA_{55}\text{-}co\text{-}PUEMA_{3.5}))_2$	19200	24600	1.18
P4	$pHPMA_{93}\text{-}co\text{-}PUEMA_7$	15700	21400	1.12
P5	$RhB\text{-}pHPMA_{58}\text{-}co\text{-}PUEMA_4$	9700	14900	1.10
C5	$CP\text{-}(RhB\text{-}pHPMA_{58}\text{-}co\text{-}PUEMA_4)_2$	20400	28300	1.13
P6	$RhB\text{-}pHPMA_{98}\text{-}co\text{-}PUEMA_8$	15700	20500	1.20

[a] Determined by ^1H NMR. [b] Determined by SEC using DMF (0.1% LiBr) as eluent, calibrated with pMMA standards.

Characterization of supramolecular nanotubes

Small angle neutron scattering (SANS) measurements were conducted on conjugates **C1-3** in aqueous solution (deuterated PBS) in order to assess their self-assembly and elucidate key structural parameters, such as shape (using the q-dependency of the scattered intensity) and dimensions (using the intensity at low q values).[47]

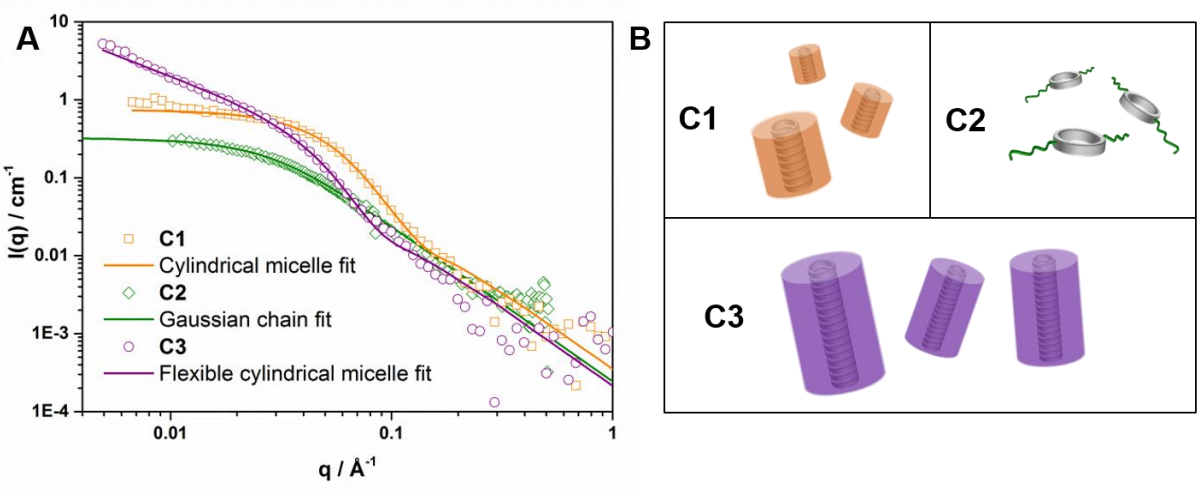

Figure 1. A) Small angle neutron scattering profiles of **C1** at 10 $mg.mL^{-1}$ (orange squares), **C2** at 5 $mg.mL^{-1}$ (green diamonds), **C3** at 5 $mg.mL^{-1}$ (purple circles) in PBS and their fits using

cylindrical micelle (orange line), Gaussian chain (green line) and flexible cylindrical micelle (purple line) models, respectively. B) Schematic representation of the three conjugates in solution.

Interestingly, all three conjugates exhibit very different scattering profiles (Figure 1A). Data for both homopolymer-based conjugates **C1** and **C2** show a plateau at low q values, indicative of a finite length, while a q^{-1} dependency is observed for **C3** in that q range, characteristic of a longer cylindrical structure. In the case of **C2**, the data is best fitted with a Gaussian chain model, which represents non-assembled polymer chains in solution (see supporting information, Table S2 and Figure S2). In contrast, models corresponding to assembled structures were necessary to fit the data corresponding to the other two conjugates. More precisely, cylindrical micelle models (worm-like) were used to fit the data for **C1** and **C3**, as they take into account both the cylindrical shape provided by the cyclic peptide core self-assembled into nanotubes (characteristic q^{-1} dependency at low q values: cylinder form factor) and the polymer arms (Gaussian chain form factor at high q values).[48] For these models, a radius of 5 Å was used for the peptide core, in accordance with previously reported results.[36] Using these parameters, reasonable values confirming the elongated shape of the structures were obtained (see supporting information, Tables S3 and S4, Figures S3 and S4). In the case of **C1** a nanotube length of about 5.2 nm was obtained, which corresponds to a aggregation number of 11, calculated using the previously reported distance between adjacent peptides[33,40] (4.7 Å).

In the case of **C3**, precise information on length could not be obtained solely using SANS, therefore static light scattering (SLS) measurements were carried out in parallel to SANS in

order to widen the window of observation and obtain scattering intensity values for lower q values (Figure 2).

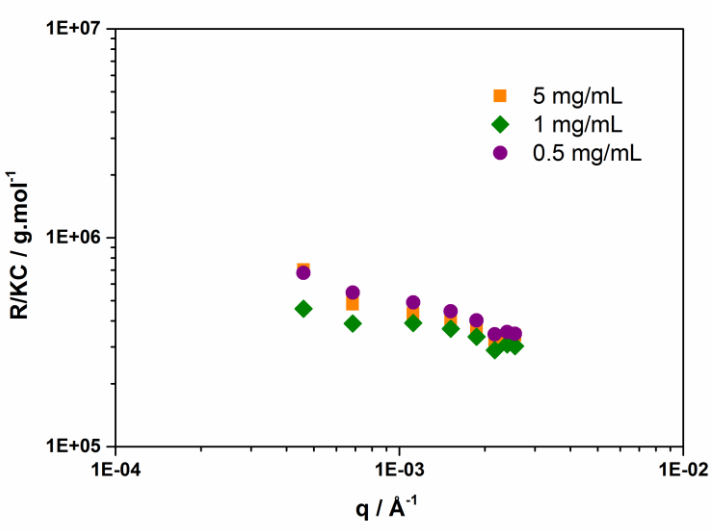

Figure 2. Static light scattering profile of **C3** (CP-(p(HPMA-*co*-PUEMA))$_2$) in solution in PBS at different concentrations.

Results show that the molecular weight of the assemblies was within the tested range independent of conjugate concentration and was found to be $6.15.10^5 \pm 0.86.10^5$ g.mol^{-1} (see Figure S5 and Table S5). These observations are in agreement with the results of Catrouillet *et al.* on self-assembling bis- and tris(urea)s decorated by polymer arms, in which the length of the obtained assemblies did not show concentration dependence, contrary to what could be expected of other supramolecular systems.[49] Using this result together with the molecular weight of the unimer and the distance between adjacent peptides, an aggregation number of 34 ± 5, and an average length of 16.0 ± 2.3 nm, were determined. The aspect ratio of these nanotubes was estimated to be around 2.9 (see supporting information). It is important to note that this value is an estimate, as it is difficult to determine the dimensions of the polymeric shell in solution with accuracy.

The noticeable difference in assembly patterns for the three conjugates (see Figure 1B for a schematic representation) is likely due to the nature of the polymers attached to the cyclic peptide, with a combination of steric hindrance and hydrogen bonding capacity influencing the stacking of the conjugates. Comparing **C1** and **C2**, which are based on different length homopolymers of HPMA (DP 25 and 53, respectively), it seems reasonable to conclude that the longer polymer chains in **C2** hindered the self-assembly process, such that the conjugate **C1** formed short cylinders (N_{agg} = 11) whereas **C2** remained as unimers in solution. This result is in line with previously reported work, which showed a decrease in tube length with increasing polymer molecular weight,[50-51] and with the general concept of frustrated growth of supramolecular systems induced by steric hindrance.[52] The differences in self-assembly between **C2** and **C3** are the most striking, since they have comparable molecular weights but contrasting morphologies in solution. The homopolymer-based **C2** did not assemble while **C3**, which contains 5% of the comonomer PUEMA, stacked into elongated tubes (N_{agg} = 34 ± 5). We attribute the differences in morphology to the presence of urea bonds and pyridine motifs in PUEMA, which provide additional hydrogen bonding and π-π stacking sites, respectively, thereby counterbalancing the steric hindrance caused by the long polymer chains, and strengthening the overall assembly.

In vitro studies

The interactions with cells of the nanotubes obtained from the self-assembly of **C3** were investigated next.. A non-self-assembling polymeric equivalent (**P4**) was synthesized in a similar manner to **P1-3** using a bifunctional CTA (see Scheme 1, Table S1 and materials and methods section for details on the synthesis,

Table 1 and Figure S1 for for SEC results).

The biocompatibility of the conjugate **C3** and the corresponding polymer control **P4** was tested *in vitro* on three cell lines (A2780 human ovarian carcinoma, PC3 human prostate carcinoma and MDA-MB-231 breast cancer) by performing cell growth inhibition assays for 72h. In all three cell lines, incubation with up to 0.5 g L^{-1} of the compounds did not result in any noticeable reduction in cell viability (Figure 3A-C).

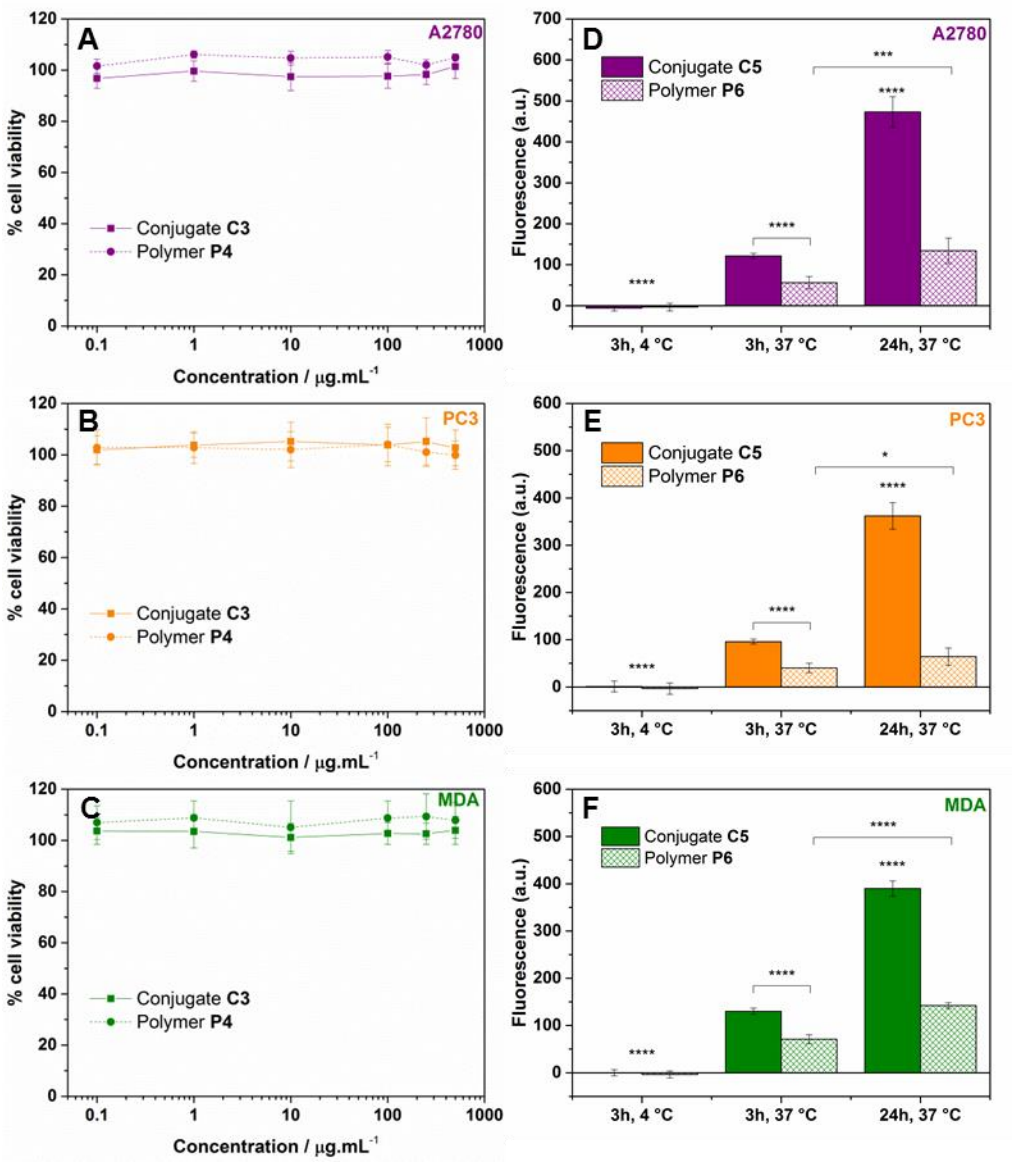

Figure 3. Toxicity profile of the compounds (continuous: conjugate, dashed: polymer) in A) A2780 B) PC3 and C) MDA cells, and cellular fluorescence intensity associated with

rhodamine as determined by flow cytometry after incubation of the compounds for 3h at 4 °C, 3h at 37 °C and 24h at 37 °C in D) A2780 E) PC3 and F) MDA cells. Data represents geometric mean of fluorescence ± SD for two independent experiments done in triplicates: *$p < 0.05$, ***$p < 0.001$, ****$p < 0.0001$.

Cellular association of the nanotubes and of the non-assembling control was subsequently quantified using flow cytometry (Figure 3D-F). To facilitate detection, a rhodamine monomer was copolymerized with HPMA and PUEMA following similar procedures to those used for the materials described above, to afford rhodamine-labelled conjugate **C5** and polymer **P6** with concentrations in rhodamine kept below 0.1 % of total monomer content (Scheme 2, see Scheme S1, Table S1 and materials and methods section for details on the synthesis, Table 1 and Figure S1 for SEC results.).

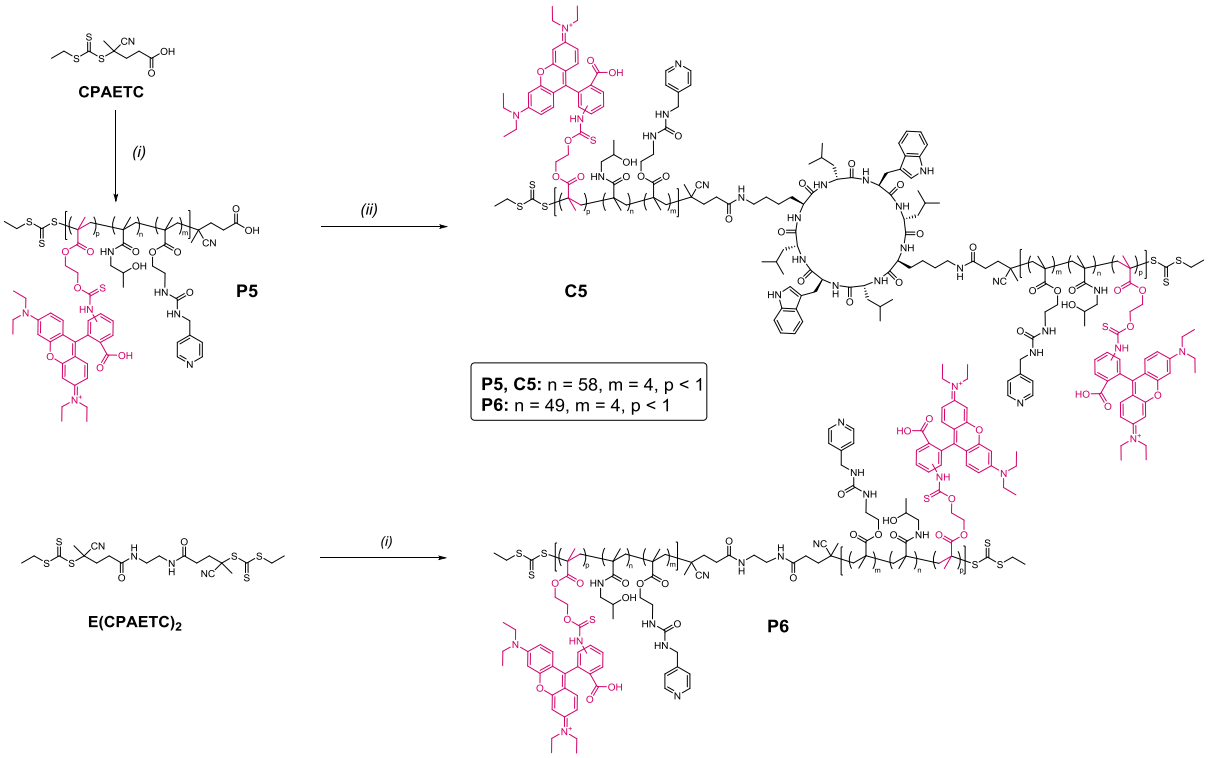

Scheme 2. Synthesis of polymer **P5,** conjugate **C5** and polymer **P6**. (*i*) HPMA, 5% PUEMA, 0.1% RhMA, VA 044, DMSO/H_2O. (*ii*) cyclo(D-Leu-Lys-D-Leu-Trp)$_2$, HBTU, NMM, DMSO.

The amount of rhodamine monomer was kept below 0.1 % of total monomer content to avoid disruption of the self-assembly process and interference with biological behaviour. Corrections factors were used to enable comparison between the two compounds, similar amounts of polymer were used in all cases and data was corrected according to fluorescence intensity (see supporting information, Figure S6 and Table S6). Cells were incubated in presence of the compounds for 3h and 24h at 37 °C. In both cases and in all three cell lines, the polymer control associated significantly less than the conjugate ($p < 0.0001$**)**. For example in A2780, the amount of conjugate **C5** measured in the cells was nearly double that of polymer **P6** after 3h; the discrepancy increased to 3.5 times more conjugate after 24h incubation. We attribute this result to the difference in size and aspect ratio between the two systems, given the fact that the conjugates self-assemble in these conditions to form a cylindrical assembly with an average aggregation number of 34, whereas the polymer **P6** remains as a single unit. Particle shape[53] and size[54-56] are thought to play a non-negligible role in cellular uptake, with larger particles exhibiting increased uptake, up to a certain size, above which the uptake generally decreases. Although results vary across studies, uptake appears to be most efficient between 20 and 100 nm, with particles with a diameter of either less than 10 nm or more than 100 nm entering the cells less than those of intermediate size. This effect is found across particles of differing nature, including coated iron oxide,[54] silica[55] and polymeric[56] nanoparticles. The present results are in line with these findings, with 16 nm-long nanotubes entering the cells to a higher extent than single polymer chains.

Cellular association increases over time, indicating that uptake occurs to a greater extent than excretion. In the case of peptide-polymer conjugate **C5**, a 3-fold increase in fluorescence in MDA cells was observed when varying the incubation time from 3h to 24h. Similar increases were found in other cell lines, with 3.8x in PC3 and 3.9x in A2780. This effect was also observed for the polymer, although to a lesser extent, and increases in fluorescence of 2.4x

between 3h and 24h incubation with A2780 cells, 1.6x with PC3 and 2.0x with MDA were recorded. In summary, these results indicate that the compounds accumulate in the cells over time (uptake > exocytosis), a phenomenon which is commonly observed for nanosized objects.[57-58]

In order to probe whether the mechanism of internalization was energy-dependent, the experiment was also performed at 4 °C, a temperature at which energy dependent uptake pathways are blocked. In all three cell lines, both compounds showed no accumulation after 3h under these conditions, suggesting that the mechanism of cellular entry relies on endocytosis or other energy-dependent pathways.

Intracellular localization of the conjugate was confirmed by confocal microscopy, using the rhodamine-labelled compound **C5** (Figure 4). Following incubation of PC3 cells with the conjugate at 20 μM for 24h, rhodamine staining inside the cells confirmed that the compound was readily taken up by the cells and not simply associated with the membrane. Control experiments are shown in supporting information (Figure S7). Lysotracker ® green was added together with the conjugate to assess organelle localization. The merged images of the red and green channels clearly demonstrate colour coincidence of the conjugate with the lysosomal compartments, which is in agreement with the flow cytometry data, suggesting uptake of the compound occurs *via* endocytosis.

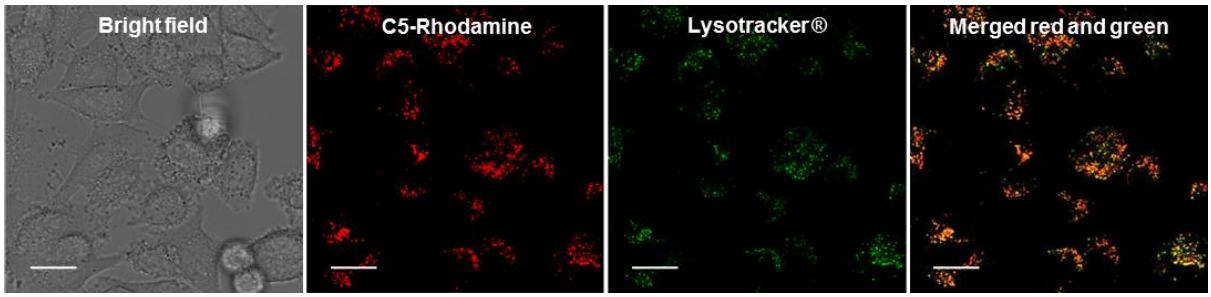

Figure 4. Confocal images of PC3 human prostate carcinoma cells treated with rhodamine-labelled conjugate **C5** for 24 h at 37 °C at a concentration of 20 μM. Lysosomes were stained using Lysotracker ® Green DND-26. Scale bar 20 μm.

Plasma pharmacokinetics and organ biodistribution

In order to quantitatively monitor the characterize the *in vivo* behaviour of the self-assembling peptide-polymer conjugates, both the conjugate **C3** and corresponding control polymer **P4** were radiolabelled, taking advantage of the hydroxyl groups present on pHPMA to attach [14C]-ethanolamine (Scheme 3). Although the extent of labelling was kept below 1% of HPMA units to avoid any potential influence of the chemical modification, we cannot completely exclude an influence of the label on self-assembly or *in vivo* behaviour of the polymers or nanotubes Nevertheless, the chemical alteration induced by the radioactive labelling is minor and is not expected to alter the physical and bio-properties of the conjugates.[59-61]

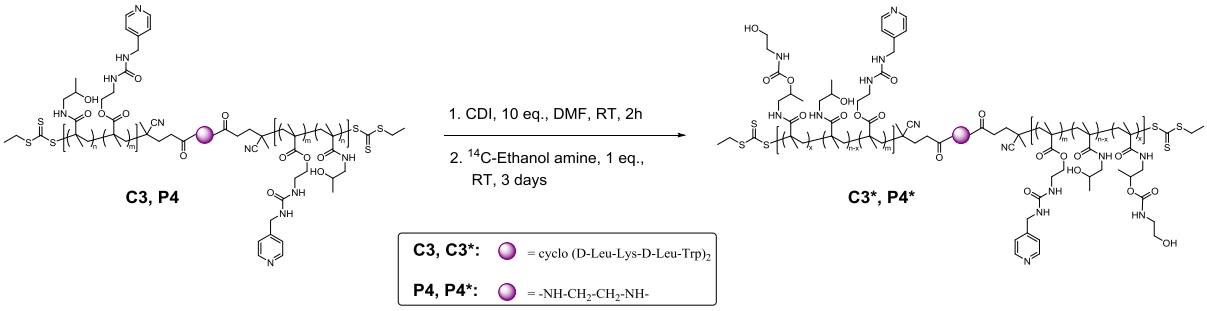

Scheme 3. Radiolabelling of compounds **C3** and **P4**.

The obtained compounds **C3*** and **P4*** were purified by size exclusion chromatography (SEC) and extensively dialysed to remove any excess radiolabel. Effective labelling was confirmed by HPLC analysis and scintillation counting of SEC fractions (Figures S8 and S9); polymer

P4* and conjugate **C3*** were found to have specific activities of 0.28 µCi/mg and 0.33 µCi/mg, respectively. The radiolabelled polymer **P4*** and conjugate **C3*** were subsequently injected intravenously to male Sprague Dawley rats at a dose of 12 $mg.kg^{-1}$ and blood samples taken at regular intervals for 24h to determine the plasma concentration *versus* time profiles (Figure 5). Taking into account the weight (~ 300 g) and blood volume (~ 20 mL) of the Sprague Dawley rats, the 12 $mg.kg^{-1}$ dose corresponds to 0.5 $mg.mL^{-1}$ at the injection time, concentration at which the conjugates are assembled into 16-nm long tubes as determined by SLS (see above).

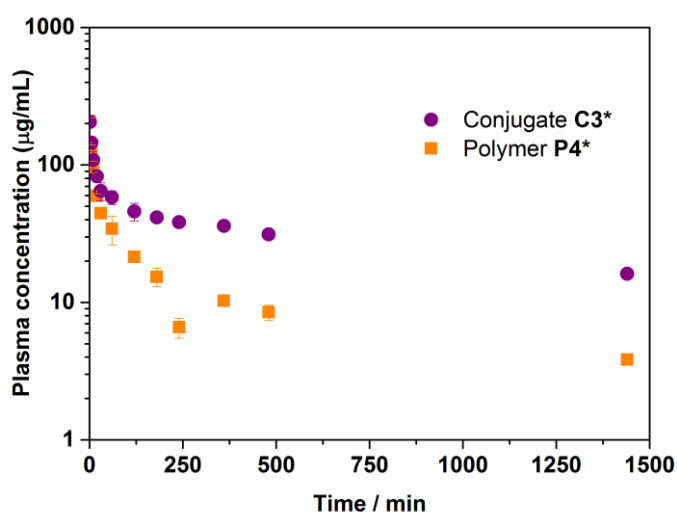

Figure 5. Plasma concentration versus time profiles of [14C]-labelled polymer **P4*** (orange squares) and conjugate **C3*** (purple circles) following intravenous administration to rats at 12 $mg.kg^{-1}$ (mean ± SD, n = 4-5 rats).

The non-compartmental (NC) pharmacokinetic parameters taken from the plasma profiles are summarized in

Table 2.

The initial volume of the central compartment (V_c) was close to blood volume, which is typical for high molecular weight materials that do not rapidly distribute out of the vasculature. The non-assembling polymer **P4*** showed relatively rapid clearance from the systemic circulation, in accordance with previously reported data for HPMA copolymers.[61-64]

In contrast, plasma exposure (AUC) of the nanotubes was significantly higher (>3 fold) than that of the polymer ($p < 0.0001$) and the increased exposure was reflected in reduced clearance (3 ± 0.2 mL.h^{-1} for the nanotubes *vs* 12 ± 0.4 mL.h^{-1} for the polymer). The terminal volume of distribution ($V_{d,\beta}$) was also significantly lower for the nanotubes (70 ± 2 mL for the nanotubes *vs* 225 ± 35 mL for the polymer chains). The combination of reductions in clearance and volume of distribution dictated that the elimination half-life of the nanotubes was relatively unchanged and only slightly longer than that of the polymer control. This parameter is calculated from the slope of the elimination phase that occurs after the rapid decrease of compound concentration during the distribution phase. In contrast to the distribution half-life, which corresponds to the distribution of compound from the blood circulation to the body tissues – it relates to drug metabolism and excretion, and is typically used to compare pharmacokinetic parameters.[65-66] We attribute the differences in systemic pharmacokinetics between polymer **P4*** and conjugate **C3*** to the larger size of the nanotubes formed by **C3***, which reduces distribution and allows them to partially avoid immediate renal clearance. The observed volume of distribution of the nanotubes is lower than for small molecular weight linear polymers, but higher than the reported values for PEGylated dendrimers (as low as 25 mL after 30h),[67] stars (approximately 60 mL after 7 days)[65] or small brushes (60 mL after 24h).[24]

Table 2. Calculated pharmacokinetic parameters and urine recovery after intravenous administration of conjugate **C3*** and polymer **P4*** to rats at 12 mg.kg^{-1} (mean ± SD, n = 4-5 rats). $^{**}p < 0.01$, $^{****}p < 0.0001$.

	Conjugate (C3*)	**Polymer (P4*)**
$t_{1/2}$ (h)	16.1 ± 1.3	13.4 ± 2.0
AUC (µg.mL^{-1}.h)	1120 ± 62	331 ± 10****
V_c (mL)	15.0 ± 1.0	16.6 ± 1.0
$V_{d,\beta}$ (mL)	70 ± 2	225 ± 35**
Cl (mL.h^{-1})	3 ± 0.2	12 ± 0.4****
Urine (% dose)	62 ± 7	72 ± 8

The percentage of dose recovery in urine after 24h was high for both the polymer chains (72 ± 8 %) and the conjugates (62 ± 7 %), indicating that the majority of both compounds is ultimately excreted from the body. The molecular weight cut-off for renal filtration is generally estimated to be around 50 kDa for hydrophilic polymers such as PEG or dextran[26] which is well below the molecular weight of the nanotubes (615 kDa, as determined by SLS) but above the mass of the polymer and the conjugate. Hence, this result suggests that the labelled compounds found in urine are fragments of the initial nanotubes, either degraded chemically (free radiolabel), or physically (unimeric conjugates or very short tubes).

In addition to the NC analysis the data was also fitted to a two-compartmental model (see materials and methods section and supporting information, Table S7 and Figure S10). Relevant pharmacokinetic parameters including $t_{1/2}$, AUC, V_d and Cl calculated from the compartmental model correlated well with those derived from the NC analysis (Table S8). In particular, the higher AUC observed for the nanotubes is maintained, with 1007 ± 153 µg.mL^{-1}.h obtained using the two-compartmental model (*vs* 1120 ± 62 µg.mL^{-1}.h using the NC model), compared to the values obtained for the polymer control (272 ± 68 µg.mL^{-1}.h and 331 ± 10 µg.mL^{-1}.h for

the two-compartmental and NC models, respectively). These results indicate confidence in the comparisons between the polymer and conjugate using either approach.

To clarify the fate of both compounds after administration, and to verify that they were both largely excreted from the body within 24h, accumulation in major organs (liver, spleen, pancreas, kidneys, heart, lungs, brain) was quantified by measuring the residual [14C] content present in the ex vivo tissues harvested 24h after IV injection. Figure 6 shows the percentage of injected [14C] recovered in each organ. Levels of accumulation were very low across all examined organs (cumulative % dose recovered < 5%), with the highest amount found in the liver (3.1 ± 0.4 % for the conjugate, 1.3 ± 0.3 % for the polymer). Note that organs were not perfused, so residual [14C] content could be due to blood, suggesting an even lower level of accumulation. Such low levels of organ accumulation are typical of small molecular weight HPMA copolymers,[64] and indicate that the compounds are either eliminated or still circulating systemically.

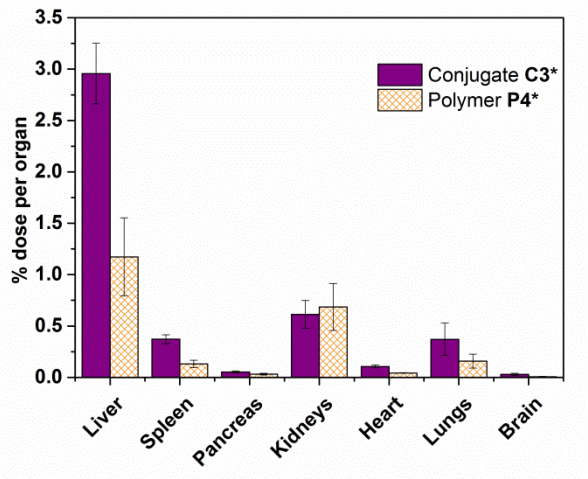

Figure 6. Distribution of [14C] in organs, 24h after intravenous administration of conjugate (purple) and polymer (orange) at 12 mg.kg^{-1} (mean ± SD, n = 4-5 rats).

The very low levels of organ uptake, together with the high urine excretion, and the intermediate value of V_d (lower than for a small molecular weight polymer but higher than for dendrimers, stars or small brushes) are consistent with the dynamic nature of the nanotubular structures. The results suggest that the peptide-polymer conjugates are initially present in plasma predominantly as the assembled nanotubes, the size of which precluded renal clearance and extravasation, but that over time disassembly results in the generation of unimeric conjugates that are more readily distributed and renally cleared, thereby avoiding organ accumulation. Nevertheless, further studies are required to more fully elucidate the mechanisms of distribution, metabolism and clearance.

Conclusions

Peptide-polymer conjugates consisting of self-assembling cyclic peptides functionalized with HPMA (co)polymers were synthesized. Assessment of their assembly properties in solution revealed the formation of nanotubes of up to 34 repeating units and ~ 16 nm in length (with an estimated aspect ratio of 2.9). Interestingly, the presence of a small fraction of a comonomer prone to non-covalent interactions greatly helped the self-assembly process. The comonomer-containing conjugate that most effectively self-assembled was tested against a non-assembling control and clear differences in cell uptake behaviour *in vitro* and pharmacokinetics *in vivo* were observed. Cellular accumulation studies demonstrated a time and temperature dependent internalization of the compounds, with the larger size of the nanotubes increasing uptake into tumour cells by a factor 3 to 4 compared to the control polymer. Confocal imaging studies confirmed accumulation of the conjugates in the lysosomal compartments of the cells, further indicating an endosomal uptake pathway. After intravenous injection to rats, conjugates were

found to circulate for 10+ hours, and to exhibit significantly lower clearance and higher plasma exposure when compared to the control polymer chains. Such characteristics may enhance passive accumulation in EPR positive tumors. Most importantly, conjugates were ultimately cleared from the systemic circulation, most likely as a result of slow disintegration of the self-assembled structures into smaller entities or even unimers. This feature of the conjugates certainly helps to avoid undesired long-term accumulation and storage diseases in organs such as the liver and spleen. Although drug induced alterations on nanotube properties need to be investigated, the present data suggest that cyclic peptide-polymer nanotubes may become a valuable type of nanosized drug delivery system.

Materials and methods

Materials

4-Aminomethyl pyridine (98%), 1-amino-2-propanol (95%), methacryloyl chloride (97%), 2-isocyanatoethyl methacrylate and deuterated solvents for NMR were purchased from Sigma-Aldrich. Potassium carbonate and anhydrous magnesium sulphate ($MgSO_4$) were purchased from Fisher Scientific. 2,2'-Azobis[2-(2-imidazolin-2-yl)propane]dihydrochloride (VA-044) was purchased from Wako Chemicals. *N*-methylmorpholine (NMM, 99 %) was purchased from Alfa Aesar. *O*-(Benzotriazole-1-yl)-*N,N,N',N'*-tetramethyluronium hexafluorophosphate (HBTU) was purchased from Iris Biotech. Methacryloxyethyl thiocarbamoyl rhodamine B (Rhodamine methacrylate, RhMA) was purchased from Polysciences. Ethanolamine [1-14C] (55 mCi/mmol, 0.1 mCi/mL) was obtained from ARC (American Radio Chemicals). All solvents were bought from commercial sources and used as received. Cyclic peptide and chain transfer agents CPAETC and $E(CPAETC)_2$ were synthesized according to previously reported protocols.[46, 68]

Characterization methods

NMR spectra were recorded on a Bruker DPX-300 instrument. Molecular weights and dispersities of polymers were assessed by size exclusion chromatography (SEC) on a Polymer Laboratories PL-GPC 50 Plus system in DMF with 0.1% LiBr, using a poly(methyl methacrylate) calibration, using refractive index detection.

SANS was carried out either on the Sans2d small angle diffractometer at the ISIS Pulsed Neutron Source (STFC Rutherford Appleton Laboratory, Didcot, UK)[69-70] or on SANS Instrument D11 at Institut Laue-Langevin in Grenoble, France.

On the Sans2d instrument, a collimation length of 4 m and incident wavelength range of 1.75 – 16.5 Å was employed. Data were measured simultaneously on two 1 m^2 detectors to give a q-range of 0.0045 – 1.00 $Å^{-1}$. The small-angle detector was positioned 4 m from the sample and offset vertically 60 mm and sideways 100 mm. The wide-angle detector was positioned 2.4 m from the sample, offset sideways by 980 mm and rotated to face the sample. The wave vector, q, is defined as:

$$q = \frac{4\pi \sin\frac{\theta}{2}}{\lambda}$$

where θ is the scattered angle and λ is the incident neutron wavelength. The beam diameter was 8 mm. Samples were prepared at a concentration of 5 mg/mL in deuterated phosphate buffer saline (PBS), and were contained in 2 mm path length quartz cells. Each raw scattering dataset was corrected for the detectors efficiencies, sample transmission and background scattering and converted to scattering cross-section data ($\partial\Sigma/\partial\Omega$ *vs.* q) using the instrument software.[71] These data were placed on an absolute scale (cm^{-1}) using the scattering from a standard sample (a solid blend of hydrogenous and perdeuterated polystyrene) in accordance with established procedures.[72]

On the D11 instrument, scattering intensities were recorded by a two-dimensional position-sensitive ^{3}He detector. Three different instrument settings were used corresponding to a wave vector $q = 4\pi \sin\frac{\theta}{2}/\lambda$ range of 0.01 < q < 0.5. H_2O was used for instrumental calibration. The data were placed on an absolute scale (cm^{-1}) using the scattering from a standard sample in accordance with established procedures.[73] The obtained reduced data was analysed with the open access software SASfit.[74]

Light scattering measurements were obtained using an ALV-CGS3 system operating with a vertically polarized laser with a wavelength of 632 nm. The measurements were taken at 20°C over a range of angles (20-150 º). The incremental refractive index, d*n*/d*C*, was determined by measuring the refractive index of the polymer in water at various concentrations ranging from 0.25 to 2 mg/mL, using a Shodex RI detector operating at a wavelength of 632 nm.

Synthetic procedures

Synthesis of 2-hydroxypropyl methacrylamide (HPMA)

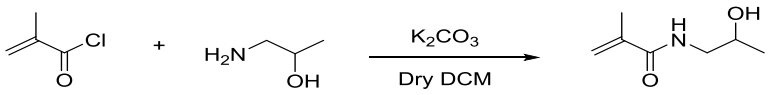

Adapted from Ulbrich *et al*.[75] Potassium carbonate (29 g, 1.1 eq., 0.21 mol) was dispersed in 120 mL of dry DCM. The mixture was cooled to -10°C with an ice-ethanol bath and 1-amino-2-propanol (14.5 mL, 1 eq., 0.19 mol) was added. Methacryloyl chloride (18.5 mL, 1 eq., 0.91 mol) was diluted with 20 mL of dry DCM, and added dropwise to the previous mixture, while maintaining the temperature at -10°C. Once the addition was complete, the reaction was left to warm up to room temperature and stirred overnight. After filtration and drying over $MgSO_4$, the DCM was evaporated and a white solid was obtained. The product was dissolved in methanol and washed with hexane, and the methanol phase was evaporated. The obtained solid was recrystallized from acetone. Yield: 45% (10.2 g). ^{1}H-NMR (d_6-DMSO, 300 MHz, ppm):

δ = 7.82 (broad s, 1H, N*H*) , 5.65 (s, 1H, C*H* vinyl), 5.31 (s, 1H, C*H* vinyl), 4.71 (s, 1H, O*H*), 3.69 (m, 1H, C*H*), 3.05 (m, 2H, CH_2), 1.85 (s, 3H, CH_2=C(CH_3)), 1.00 (d, *J* = 6 Hz, 3H, CH-CH_3). ^{13}C-DEPT-NMR (d_6-DMSO, 75 MHz, ppm): δ = 167.7, 139.9, 118.9, 85.1, 46.7, 21.1, 18.6.

Synthesis of 2-(3-(pyridin-4-ylmethyl)ureido)ethyl)methacrylate (PUEMA)

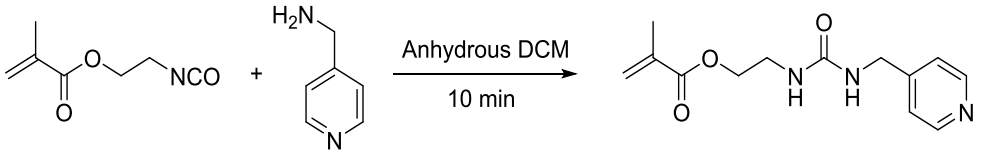

2-Isocyanatoethyl methacrylate (2.2 g, 14.15 mmol) and 4-aminomethyl pyridine (1.53 g, 1 eq., 14.15 mmol) were mixed in dry DCM (10 mL) and left to stir at room temperature for 10 min. The solvent was evaporated under reduced pressure and PUEMA was collected as a white powder. Yield: 95% (3.53 g). ^{1}H-NMR ($CDCl_3$, 300 MHz, ppm): δ = 8.52 (d, 2H, C*H*-N-C*H* pyridine), 7.19 (d, 2H, C*H*-C-C*H* pyridine), 6.09 (s, 1H, C*H* vinyl), 5.59 (s, 1H, C*H* vinyl), 5.13 (broad t, 1H, N*H* urea), 4.97 (broad t, 1H, N*H* urea), 4.38 (d, 2H, NH-CH_2-pyridine), 4.25 (t, 2H, O-CH_2), 3.53 (q, 2H, O-CH_2-CH_2), 1.93 (s, 3H, CH_3). ^{13}C-DEPT-NMR ($CDCl_3$, 75 MHz, ppm): 166.9, 157.5, 149.2, 148.3, 135.3, 125.5, 121.4, 63.4, 42.4, 39.0, 17.6. FTIR: (ν, cm^{-1}): 3313 (N-H stretch, urea), 1720 (C=O stretch, methacrylate), 1623 (C=C stretch, alkene), 1585 (C=O stretch, urea). MS (ESI): $[M+Na]^+$ calculated: 286.1, found: 285.9.

RAFT polymer synthesis

Chain transfer agent (CTA, here CPAETC or E(CPAETC)$_2$), monomers (HPMA, PUEMA, RhMA), initiator (VA 044) and solvent (70/30 DMSO/H_2O) were introduced into a flask equipped with a magnetic stirrer and sealed with a rubber septum (see Table S1 for detailed conditions). The solution was degassed by bubbling nitrogen through it for 15 min, and then

put in an oil bath at 44°C for the indicated time. Conversions were determined by ^{1}H NMR. For polymers **P5** and **P6**, conversion of RhMA could not be determined because the extremely low amounts did not allow visualization of the corresponding signals. The polymers were precipitated in ice-cold acetone and dried under vacuum. The rhodamine-labelled polymers **P5** and **P6** were further dialysed to remove any excess dye.

Conjugation of polymers to the cyclic peptide

General protocol: cyclic peptide, polymer (2.5 eq.) and HBTU (3.75 eq.) were solubilized in DMSO (1.5 mL). NMM (6 eq.) was added and the reaction mixture was left to stir at room temperature for 2 hours. After the reaction, DMSO was removed using a stream of N_2 and the conjugates were dissolved in water and purified from the excess polymer using a centrifugal ultrafiltration unit with a molecular weight cut off of 30 kDa (Amicon® Ultra centrifugal filter). The isolated conjugates were freeze-dried.

Radiolabelling of compounds

Conjugate **C3** (or polymer **P4**) was introduced in a vial, together with CDI (10 eq.) and anhydrous DMF (1 mL) and the mixture was stirred for 4 hours. An aliquot of [14C]-labelled ethanolamine in ethanol was withdrawn from the bottle (1 eq.) and the ethanol evaporated using a steam of nitrogen. DMF was used to redissolve the radiolabel and add it to the mixture, which was then stirred for 4 days. The solvent was removed using a stream of nitrogen and the dried-up mixture was solubilized in water and passed over a size exclusion column (PD10, GE Healthcare Life Sciences) to remove most of the remaining free radiolabel prior to dialysis. The purity of the radiolabelled compounds **C3*** and **P4*** was assessed by HPLC and size exclusion chromatography using PD10 cartridges (Figures S8-9). Briefly, 0.7 mL fractions were collected and the activity of each fraction was determined by scintillation counting.

In vitro testing

Cells

A2780 (human ovarian carcinoma), PC3 (human prostate carcinoma) and MDA-MB-231 (human breast cancer) cells were obtained either from the European Collection of Cell Cultures (ECACC) or Sigma-Aldrich. A2780 were grown in Roswell Park Memorial Institute medium (RPMI-1640), and PC3 and MDA-MB-231 in Dulbecco's Modified Eagle Medium (DMEM). Both media were supplemented with 10% v/v of foetal calf serum, 1% v/v of 2 mM glutamine and 1% v/v penicillin/streptomycin. Cells were grown as adherent monolayers at 37 °C in a 5% CO_2 humidified atmosphere and passaged at approximately 70-80% confluence.

Growth inhibition assay

Briefly, 5000 cells were seeded per well in 96-well plates and allowed to grow for 24 h before adding different concentrations of the compounds to be tested. Compounds were dissolved directly in cell culture medium at concentrations ranging from 0.1 to 500 μg/mL. Culture medium was replaced by dilutions of the compounds and cells further incubated for 72 h. After this, supernatant was removed and replaced by fresh medium. XTT assay was used to determine cell viability. Absorbance measurements of the plate at 475 nm were carried out using a Synergy HTX (Biotek) plate reader. Determination of viable treated cells was done in comparison to untreated controls. Two independent sets of experiments in triplicates were carried out and standard deviations were used for error bars.

Microscopy

Cells were seeded in an 8-chamber imaging plate (Eppendorf) at 15000 cells per well and incubated overnight at 37 °C with 5% CO_2. Rhodamine-labelled conjugate dissolved in PBS was added to the wells to a final concentration of 20 μM and incubated for 24 h. Colocalization studies were carried out after lysosome staining using Lysotracker® Green DND-26. Labelling

was achieved by incubating cells in the presence of Lysotracker (100 nM) for 2 hours. The cells were washed 2 times with fresh media and images were recorded using a Leica SP5 Laser-scanning confocal microscope with a HCX PL APO 40x (NA 1.25) oil objective. Images were acquired at 1024x1024, capturing rhodamine (ex 561; em: 565-580 nm), lysotracker GFP (ex 488; em 504-520 nm) and transmission channels. Image acquisition settings were consistent for samples and controls.

Flow cytometry

Cells were seeded in 24-well plates at 100 000 cells per well and incubated in 500 µL of compound-free media overnight at 37 °C with 5% CO_2. Rhodamine-labelled compounds were then added to cells in triplicate, achieving a final concentration of 20 µM. Three sets of conditions were tested: incubation at 37 °C for 24 h, incubation at 37 °C for 3 h, and incubation at 4 °C for 3 h. For the incubation at 4 °C, the cells were placed on ice for 10 min prior to addition of the compound, and subsequently in the fridge. After incubation, the culture medium was removed, and the cells were washed with PBS, harvested with trypsin, transferred to Eppendorf tubes and spun at 1500 g for 5 min. The supernatant was discarded and cell pellets were resuspended in PBS, transferred into flow cytometry tubes and stocked on ice until measurement. Samples were analysed on a BD FACScan flow cytometer using the FL2 channel (585/42 nm). Cells were analysed using forward and side scatter gates to exclude debris and cell aggregates. Fluorescence intensity corresponding to untreated cells was subtracted, the data were processed using Flowing software 2® and reported values correspond to the average of the means of fluorescence for a population of 10000 cells.

Activity Determination and Scintillation Counting

The specific activity of the compounds was determined by dilution of known amounts of material into PBS. Aliquots were mixed with 4 mL of Ultima Gold and scintillation counted

on a Packard Tri-Carb 2000CA liquid scintillation analyzer (Meriden, CT). Polymer **P4*** and conjugate **C3*** were found to have specific activities of 0.28 μCi/mg and 0.33 μCi/mg, respectively.

Pharmacokinetics and Biodistribution studies

Animals

All animal experimental protocols were approved by the Monash Institute of Pharmaceutical Sciences Animal Ethics Committee, Monash University, Parkville, VIC, Australia. Male Sprague Dawley rats (250-350 g) were used in these experiments. Animals were maintained on a 12h light/dark cycle at all times.

Intravenous Pharmacokinetic Studies

A day prior to compound administration, each rat was anaesthetised under isoflurane (2-5% v/v) and cannulas (polyethylene tubing 0.96 x 0.58 mm, Paton Scientific, Victor Harbour, Australia) surgically inserted into the right jugular vein and carotid artery (to facilitate IV administration and blood collection respectively) as previously described.[76] The rats were transferred to individual metabolic cages (to permit separate collection of urine and faeces) and allowed to recover overnight prior to dosing. Each animal was fasted up to 14h prior to and up to 8h after administration of the IV dose with water provided *ad libitum*. Prior to injection, blank blood samples (0.2 mL) were obtained from the carotid artery. The compounds were dissolved in phosphate buffered saline (PBS) and 0.5 mL was administered at a dose of 12 mg/kg as a slow bolus intravenous injection (1 mL/min) via the jugular cannula. The cannula was then flushed with 0.5 mL of heparinized saline to ensure complete infusion of the dose. Subsequent blood samples (0.2 mL) were taken at 1, 5, 10, 20, 30, 60, 120, 180, 240, 360, 480, and 1440 min after dose administration. Blood samples were placed immediately into tubes containing 10 IU of heparin and centrifuged for 5 min at 3500*g*. Plasma (0.1 mL) was collected,

transferred to a separate vial and mixed with 4 mL of Ultima Gold scintillation cocktail prior to scintillation counting.

Biodistribution Studies

At the end of the pharmacokinetic studies (24h), animals were humanely killed by injection of a lethal dose of sodium pentobarbital (via the jugular vein cannula) and the following tissues removed: liver, spleen, pancreas, kidneys, heart, lungs and brain. The tissues were frozen (-20 °C) and stored in pre-weighed polypropylene tubes until processing and analysis. The samples were homogenized using a gentleMACS Dissociator (Miltenyi Biotech) with 5 mL of MilliQ water. Triplicate samples from each tissue homogenate (typically 50-100 mg of tissue) were mixed with 2 mL of Solvable (Perkin Elmer) and the samples placed at 60 °C overnight to facilitate tissue digestion. The samples were cooled to room temperature and 200 µL hydrogen peroxide (30% w/v) were added to each vial. Samples were left open at room temperature until bubbling had ceased. Ultima Gold (10 mL) was then added and the mixture vortexed before the samples were stored at 4 °C in the dark, without agitation, for at least 3 days prior to scintillation counting. Blank organs also were treated as above to provide for background correction. In order to correct for any reduction in radioactivity counting efficacy due to the processing of the tissues, an identical second set of samples was processed in the same way but the tissue homogenate aliquots were spiked with a known quantity of radiolabel prior to addition of Solvable. All samples were then scintillation counted at 12 °C.

A processing efficiency was calculated, using the following equation:

$$efficiency = \frac{spiked\ tissue_{dpm} - tissue_{dpm,uncorr}}{spiked\ solution_{dpm}}$$

Where spiked $tissue_{dpm}$ was the mass-corrected radioactivity measured in the spiked samples, $tissue_{dpm,uncorr}$ was the mass-corrected radioactivity in the non-spiked tissue samples, and spiked $soln_{dpm}$ was the known amount of radioactivity added to the spiked sample. Effectively, the calculation provides an indication of the efficiency of counting, using the known (spiked)

amount of radioactivity in each tissue as a reference. This value for efficiency was used to correct the [14C] content in the processed sample using the following equation:

$$tissue_{dpm,corr} = \frac{tissue_{dpm,uncorr}}{efficiency}$$

The activity in the whole organ was then calculated knowing the mass fraction of the entire organ present in the processed sample. The results are expressed as either the percentage of injected dose in the organ at sacrifice or the percentage of injected dose per gram of tissue.

Urine

Urine, pooled from immediately after dose administration till 24h, was collected at the end of the study. A blank urine sample was also collected to provide for background correction. After accounting for the volume of pooled urine collected a 100 μL aliquot was taken and mixed with 4 mL of Ultima Gold and scintillation counted. After background subtraction, the radiolabel content of the sample was corrected for the total volume of urine collected and converted to a percentage of the total administered dose.

Calculation of Pharmacokinetic Parameters

The concentrations of radiolabel in plasma/whole blood samples were converted to microgram equivalent concentrations using the specific activity of the radiolabeled compounds. Non-compartmental pharmacokinetic parameters were calculated with Excel using the PK solver add-in.[77] The NCA IV Bolus model was used, in which the $AUC_{0-\infty}$ was calculated using the linear trapezoidal method. The elimination half-life ($t_{1/2}$), volume of distribution (V_d) and clearance (Cl) were also determined from the model. An estimate of initial distribution volume, or volume of central compartment (V_c) was calculated from the dose/Cp^0, where Cp^0 was the extrapolated concentration in plasma at the moment of completion of the injection. In addition to the non compartmental analysis the data was also fitted to a two-compartmental model and analysed using Phoenix WinNonlin software (Version 6.3, Cetara). Plasma profiles fitted to

the two-compartment model and derived PK parameters are provided in Supporting Information.

Associated content

Supporting Information available: details on synthesis (schemes and polymerization conditions), SANS and SLS analyses, additional characterization (SEC, HPLC, determination of fluorescence correction factors), complementary pharmacokinetics analysis.

Acknowledgements

"This project has received funding from the European Research Council (ERC) under the European Union's Horizon 2020 research and innovation programme (grant agreement No 647106)". We thank the Royal Society Wolfson Merit Award (WM130055; SP), the Monash-Warwick Alliance (SL; SP) and the ARC (DP140100241; KAJ; SP) for financial support. JB thanks the German Science Foundation (DFG) for granting a full postdoctoral fellowship (BR 4905/1-1). We thank ISIS and Institut Laue Langevin (ILL) for neutron scattering beam time, Dr Sarah Rodgers (ISIS) and Dr. Peter Lindner (ILL) for instrument training and support. SL acknowledges G. Gracia, G. Lee and I. Styles for their support in the animal lab.

References

(1) Hoffman, A. S., The origins and evolution of "controlled" drug delivery systems. *J. Controlled Release* **2008,** *132* (3), 153-163.
(2) Cho, K.; Wang, X.; Nie, S.; Chen, Z.; Shin, D. M., Therapeutic Nanoparticles for Drug Delivery in Cancer. *Clinical Cancer Research* **2008,** *14* (5), 1310-1316.
(3) Maeda, H., Tumor-Selective Delivery of Macromolecular Drugs via the EPR Effect: Background and Future Prospects. *Bioconjugate Chem.* **2010,** *21* (5), 797-802.
(4) Maeda, H.; Nakamura, H.; Fang, J., The EPR effect for macromolecular drug delivery to solid tumors: Improvement of tumor uptake, lowering of systemic toxicity, and distinct tumor imaging in vivo. *Adv. Drug Delivery Rev.* **2013,** *65* (1), 71-79.

(5) Pasut, G.; Veronese, F. M., State of the art in PEGylation: The great versatility achieved after forty years of research. *J. Controlled Release* **2012,** *161* (2), 461-472.
(6) Nicolas, J.; Mura, S.; Brambilla, D.; Mackiewicz, N.; Couvreur, P., Design, functionalization strategies and biomedical applications of targeted biodegradable/biocompatible polymer-based nanocarriers for drug delivery. *Chem. Soc. Rev.* **2013,** *42* (3), 1147-1235.
(7) Chou, L. Y. T.; Ming, K.; Chan, W. C. W., Strategies for the intracellular delivery of nanoparticles. *Chem. Soc. Rev.* **2011,** *40* (1), 233-245.
(8) Kamaly, N.; Xiao, Z. Y.; Valencia, P. M.; Radovic-Moreno, A. F.; Farokhzad, O. C., Targeted polymeric therapeutic nanoparticles: design, development and clinical translation. *Chem. Soc. Rev.* **2012,** *41* (7), 2971-3010.
(9) Ghosh, P.; Han, G.; De, M.; Kim, C. K.; Rotello, V. M., Gold nanoparticles in delivery applications. *Adv. Drug Delivery Rev.* **2008,** *60* (11), 1307-1315.
(10) Probst, C. E.; Zrazhevskiy, P.; Bagalkot, V.; Gao, X., Quantum dots as a platform for nanoparticle drug delivery vehicle design. *Adv. Drug Delivery Rev.* **2013,** *65* (5), 703-718.
(11) Argyo, C.; Weiss, V.; Bräuchle, C.; Bein, T., Multifunctional Mesoporous Silica Nanoparticles as a Universal Platform for Drug Delivery. *Chem. Mater.* **2014,** *26* (1), 435-451.
(12) Allen, T. M.; Cullis, P. R., Liposomal drug delivery systems: From concept to clinical applications. *Adv. Drug Delivery Rev.* **2013,** *65* (1), 36-48.
(13) Sharma, A.; Sharma, U. S., Liposomes in drug delivery: Progress and limitations. *Int. J. Pharm.* **1997,** *154* (2), 123-140.
(14) Kaneda, Y.; Nakajima, T.; Nishikawa, T.; Yamamoto, S.; Ikegami, H.; Suzuki, N.; Nakamura, H.; Morishita, R.; Kotani, H., Hemagglutinating Virus of Japan (HVJ) Envelope Vector as a Versatile Gene Delivery System. *Molecular Therapy* **2002,** *6* (2), 219-226.
(15) Liu, Z.; Chen, K.; Davis, C.; Sherlock, S.; Cao, Q.; Chen, X.; Dai, H., Drug Delivery with Carbon Nanotubes for *In vivo* Cancer Treatment. *Cancer Research* **2008,** *68* (16), 6652-6660.
(16) Liechty, W. B.; Kryscio, D. R.; Slaughter, B. V.; Peppas, N. A., Polymers for drug delivery systems. *Annual review of chemical and biomolecular engineering* **2010,** *1*, 149-173.
(17) Venkataraman, S.; Hedrick, J. L.; Ong, Z. Y.; Yang, C.; Ee, P. L. R.; Hammond, P. T.; Yang, Y. Y., The effects of polymeric nanostructure shape on drug delivery. *Adv. Drug Delivery Rev.* **2011,** *63* (14–15), 1228-1246.
(18) Truong, N. P.; Whittaker, M. R.; Mak, C. W.; Davis, T. P., The importance of nanoparticle shape in cancer drug delivery. *Expert Opinion on Drug Delivery* **2015,** *12* (1), 129-142.
(19) Geng, Y.; Dalhaimer, P.; Cai, S. S.; Tsai, R.; Tewari, M.; Minko, T.; Discher, D. E., Shape effects of filaments versus spherical particles in flow and drug delivery. *Nat. Nanotechnol.* **2007,** *2* (4), 249-255.
(20) Müllner, M., Molecular Polymer Brushes in Nanomedicine. *Macromol. Chem. Phys.* **2016,** *217* (20), 2209-2222.
(21) Schlick, T. L.; Ding, Z.; Kovacs, E. W.; Francis, M. B., Dual-Surface Modification of the Tobacco Mosaic Virus. *J. Am. Chem. Soc.* **2005,** *127* (11), 3718-3723.
(22) Bruckman, M. A.; Randolph, L. N.; VanMeter, A.; Hern, S.; Shoffstall, A. J.; Taurog, R. E.; Steinmetz, N. F., Biodistribution, pharmacokinetics, and blood compatibility of native and PEGylated tobacco mosaic virus nano-rods and -spheres in mice. *Virology* **2014,** *449*, 163-173.
(23) Christian, D. A.; Cai, S.; Garbuzenko, O. B.; Harada, T.; Zajac, A. L.; Minko, T.; Discher, D. E., Flexible Filaments for in vivo Imaging and Delivery: Persistent Circulation of Filomicelles Opens the Dosage Window for Sustained Tumor Shrinkage. *Mol. Pharmaceutics* **2009,** *6* (5), 1343-1352.
(24) Müllner, M.; Dodds, S. J.; Nguyen, T.-H.; Senyschyn, D.; Porter, C. J. H.; Boyd, B. J.; Caruso, F., Size and Rigidity of Cylindrical Polymer Brushes Dictate Long Circulating Properties In Vivo. *ACS Nano* **2015,** *9* (2), 1294-1304.
(25) Mullner, M.; Mehta, D.; Nowell, C. J.; Porter, C. J. H., Passive tumour targeting and extravasation of cylindrical polymer brushes in mouse xenografts. *Chem. Commun.* **2016,** *52* (58), 9121-9124.

(26) Elsabahy, M.; Wooley, K. L., Design of polymeric nanoparticles for biomedical delivery applications. *Chem. Soc. Rev.* **2012,** *41* (7), 2545-2561.
(27) Branco, M. C.; Schneider, J. P., Self-assembling materials for therapeutic delivery. *Acta Biomaterialia* **2009,** *5* (3), 817-831.
(28) Otter, R.; Klinker, K.; Spitzer, D.; Schinnerer, M.; Barz, M.; Besenius, P., Folding induced supramolecular assembly into pH-responsive nanorods with a protein repellent shell. *Chem. Commun.* **2018,** *54* (4), 401-404.
(29) Klinker, K.; Schäfer, O.; Huesmann, D.; Bauer, T.; Capelôa, L.; Braun, L.; Stergiou, N.; Schinnerer, M.; Dirisala, A.; Miyata, K.; Osada, K.; Cabral, H.; Kataoka, K.; Barz, M., Secondary‐Structure‐Driven Self‐Assembly of Reactive Polypept(o)ides: Controlling Size, Shape, and Function of Core Cross‐Linked Nanostructures. *Angew. Chem. Int. Ed.* **2017,** *56* (32), 9608-9613.
(30) Aida, T.; Meijer, E. W.; Stupp, S. I., Functional Supramolecular Polymers. *Science* **2012,** *335* (6070), 813.
(31) Krieg, E.; Bastings, M. M. C.; Besenius, P.; Rybtchinski, B., Supramolecular Polymers in Aqueous Media. *Chem. Rev.* **2016,** *116* (4), 2414-2477.
(32) Zhang, J.; Ma, P. X., Cyclodextrin-based supramolecular systems for drug delivery: Recent progress and future perspective. *Adv. Drug Delivery Rev.* **2013,** *65* (9), 1215-1233.
(33) Hartgerink, J. D.; Beniash, E.; Stupp, S. I., Self-Assembly and Mineralization of Peptide-Amphiphile Nanofibers. *Science* **2001,** *294* (5547), 1684-1688.
(34) Matson, J. B.; Stupp, S. I., Drug release from hydrazone-containing peptide amphiphiles. *Chem. Commun.* **2011,** *47* (28), 7962-7964.
(35) Soukasene, S.; Toft, D. J.; Moyer, T. J.; Lu, H.; Lee, H.-K.; Standley, S. M.; Cryns, V. L.; Stupp, S. I., Anti-Tumor Activity of Peptide Amphiphile Nanofiber-Encapsulated Camptothecin. *ACS Nano* **2011,** *5* (11), 9113-9121.
(36) Chapman, R.; Danial, M.; Koh, M. L.; Jolliffe, K. A.; Perrier, S., Design and properties of functional nanotubes from the self-assembly of cyclic peptide templates. *Chem. Soc. Rev.* **2012,** *41* (18), 6023-6041.
(37) Ghadiri, M. R.; Granja, J. R.; Milligan, R. A.; McRee, D. E.; Khazanovich, N., Self-assembling organic nanotubes based on a cyclic peptide architecture. *Nature* **1993,** *366* (6453), 324-327.
(38) Blunden, B. M.; Chapman, R.; Danial, M.; Lu, H. X.; Jolliffe, K. A.; Perrier, S.; Stenzel, M. H., Drug Conjugation to Cyclic Peptide-Polymer Self-Assembling Nanotubes. *Chem. Eur. J.* **2014,** *20* (40), 12745-12749.
(39) Wang, Y.; Yi, S.; Sun, L.; Huang, Y.; Lenaghan, S. C.; Zhang, M., Doxorubicin-Loaded Cyclic Peptide Nanotube Bundles Overcome Chemoresistance in Breast Cancer Cells. *J. Biomed. Nanotechnol.* **2014,** *10* (3), 445-454.
(40) Larnaudie, S. C.; Brendel, J. C.; Romero-Canelón, I.; Sanchez-Cano, C.; Catrouillet, S.; Sanchis, J.; Coverdale, J. P. C.; Song, J.-I.; Habtemariam, A.; Sadler, P. J.; Jolliffe, K. A.; Perrier, S., Cyclic peptide-polymer nanotubes as efficient and highly potent drug delivery systems for organometallic anticancer complexes. *Biomacromolecules* **2017**.
(41) Kopeček, J.; Kopečková, P., HPMA copolymers: Origins, early developments, present, and future. *Adv. Drug Delivery Rev.* **2010,** *62* (2), 122-149.
(42) Duncan, R., Polymer conjugates as anticancer nanomedicines. *Nat. Rev. Cancer* **2006,** *6* (9), 688-701.
(43) Sanchis, J.; Canal, F.; Lucas, R.; Vicent, M. J., Polymer-drug conjugates for novel molecular targets. *Nanomedicine* **2010,** *5* (6), 915-935.
(44) Danial, M.; Tran, C. M. N.; Jolliffe, K. A.; Perrier, S., Thermal Gating in Lipid Membranes Using Thermoresponsive Cyclic Peptide-Polymer Conjugates. *J. Am. Chem. Soc.* **2014,** *136* (22), 8018-8026.
(45) Danial, M.; Tran, C. M. N.; Young, P. G.; Perrier, S.; Jolliffe, K. A., Janus cyclic peptide-polymer nanotubes. *Nat. Commun.* **2013,** *4*, 2780.
(46) Larnaudie, S. C.; Brendel, J. C.; Jolliffe, K. A.; Perrier, S., Cyclic peptide–polymer conjugates: Grafting-to vs grafting-from. *J. Polym. Sci., Part A: Polym. Chem.* **2016,** *54* (7), 1003-1011.

(47) Perrier, S.; Barlow, T.; Catrouillet, S.; Gurnani, P.; Kerr, A.; Koh, M. L.; Larnaudie, S.; Rho, J.; Schweins, R.; Lindner, P.; Warr, G., Elucidation and control over the self-assembly of (cyclic peptide)-polymer conjugates. . *Institut Laue-Langevin (ILL), doi:10.5291/ILL-DATA.9-10-1412* **2015**.
(48) Pedersen, J. S., Form factors of block copolymer micelles with spherical, ellipsoidal and cylindrical cores. *J. Appl. Crystallogr.* **2000,** *33* (1), 637-640.
(49) Catrouillet, S.; Fonteneau, C.; Bouteiller, L.; Delorme, N.; Nicol, E.; Nicolai, T.; Pensec, S.; Colombani, O., Competition Between Steric Hindrance and Hydrogen Bonding in the Formation of Supramolecular Bottle Brush Polymers. *Macromolecules* **2013,** *46* (19), 7911-7919.
(50) Couet, J.; Biesalski, M., Polymer-Wrapped Peptide Nanotubes: Peptide-Grafted Polymer Mass Impacts Length and Diameter. *Small* **2008,** *4* (7), 1008-1016.
(51) Chapman, R.; Jolliffe, K. A.; Perrier, S., Modular design for the controlled production of polymeric nanotubes from polymer/peptide conjugates. *Polym. Chem.* **2011,** *2* (9), 1956-1963.
(52) Appel, R.; Fuchs, J.; Tyrrell, S. M.; Korevaar, P. A.; Stuart, M. C. A.; Voets, I. K.; Schönhoff, M.; Besenius, P., Steric Constraints Induced Frustrated Growth of Supramolecular Nanorods in Water. *Chem. Eur. J.* **2015,** *21* (52), 19257-19264.
(53) Huang, X.; Teng, X.; Chen, D.; Tang, F.; He, J., The effect of the shape of mesoporous silica nanoparticles on cellular uptake and cell function. *Biomaterials* **2010,** *31* (3), 438-448.
(54) Huang, J.; Bu, L.; Xie, J.; Chen, K.; Cheng, Z.; Li, X.; Chen, X., Effects of Nanoparticle Size on Cellular Uptake and Liver MRI with Polyvinylpyrrolidone-Coated Iron Oxide Nanoparticles. *ACS Nano* **2010,** *4* (12), 7151-7160.
(55) Lu, F.; Wu, S.-H.; Hung, Y.; Mou, C.-Y., Size Effect on Cell Uptake in Well-Suspended, Uniform Mesoporous Silica Nanoparticles. *Small* **2009,** *5* (12), 1408-1413.
(56) Yin Win, K.; Feng, S.-S., Effects of particle size and surface coating on cellular uptake of polymeric nanoparticles for oral delivery of anticancer drugs. *Biomaterials* **2005,** *26* (15), 2713-2722.
(57) Kulkarni, S. A.; Feng, S.-S., Effects of Particle Size and Surface Modification on Cellular Uptake and Biodistribution of Polymeric Nanoparticles for Drug Delivery. *Pharm. Res.* **2013,** *30* (10), 2512-2522.
(58) Hinde, E.; Thammasiraphop, K.; Duong, H. T. T.; Yeow, J.; Karagoz, B.; Boyer, C.; Gooding, J. J.; Gaus, K., Pair correlation microscopy reveals the role of nanoparticle shape in intracellular transport and site of drug release. *Nat Nano* **2016,** *advance online publication*.
(59) Lammers, T.; Peschke, P.; Kühnlein, R.; Subr, V.; Ulbrich, K.; Debus, J.; Huber, P.; Hennink, W.; Storm, G., Effect of radiotherapy and hyperthermia on the tumor accumulation of HPMA copolymer-based drug delivery systems. *J. Controlled Release* **2007,** *117* (3), 333-341.
(60) Allmeroth, M.; Moderegger, D.; Gündel, D.; Buchholz, H.-G.; Mohr, N.; Koynov, K.; Rösch, F.; Thews, O.; Zentel, R., PEGylation of HPMA-based block copolymers enhances tumor accumulation in vivo: A quantitative study using radiolabeling and positron emission tomography. *J. Controlled Release* **2013,** *172* (1), 77-85.
(61) Herth, M. M.; Barz, M.; Moderegger, D.; Allmeroth, M.; Jahn, M.; Thews, O.; Zentel, R.; Rösch, F., Radioactive Labeling of Defined HPMA-Based Polymeric Structures Using [18F]FETos for In Vivo Imaging by Positron Emission Tomography. *Biomacromolecules* **2009,** *10* (7), 1697-1703.
(62) Etrych, T.; Kovář, L.; Strohalm, J.; Chytil, P.; Říhová, B.; Ulbrich, K., Biodegradable star HPMA polymer–drug conjugates: Biodegradability, distribution and anti-tumor efficacy. *J. Controlled Release* **2011,** *154* (3), 241-248.
(63) Etrych, T.; Šubr, V.; Strohalm, J.; Šírová, M.; Říhová, B.; Ulbrich, K., HPMA copolymer-doxorubicin conjugates: The effects of molecular weight and architecture on biodistribution and in vivo activity. *J. Controlled Release* **2012,** *164* (3), 346-354.
(64) Sadekar, S.; Ray, A.; Janàt-Amsbury, M.; Peterson, C. M.; Ghandehari, H., Comparative Biodistribution of PAMAM Dendrimers and HPMA Copolymers in Ovarian-Tumor-Bearing Mice. *Biomacromolecules* **2011,** *12* (1), 88-96.
(65) Khor, S. Y.; Hu, J.; McLeod, V. M.; Quinn, J. F.; Williamson, M.; Porter, C. J. H.; Whittaker, M. R.; Kaminskas, L. M.; Davis, T. P., Molecular weight (hydrodynamic volume) dictates the systemic

pharmacokinetics and tumour disposition of PolyPEG star polymers. *Nanomedicine: Nanotechnology, Biology and Medicine* **2015,** *11* (8), 2099-2108.
(66) Kaminskas, L. M.; Boyd, B. J.; Karellas, P.; Krippner, G. Y.; Lessene, R.; Kelly, B.; Porter, C. J. H., The Impact of Molecular Weight and PEG Chain Length on the Systemic Pharmacokinetics of PEGylated Poly l-Lysine Dendrimers. *Mol. Pharmaceutics* **2008,** *5* (3), 449-463.
(67) Kaminskas, L. M.; Kelly, B. D.; McLeod, V. M.; Boyd, B. J.; Krippner, G. Y.; Williams, E. D.; Porter, C. J. H., Pharmacokinetics and Tumor Disposition of PEGylated, Methotrexate Conjugated Poly-l-lysine Dendrimers. *Mol. Pharmaceutics* **2009,** *6* (4), 1190-1204.
(68) Catrouillet, S.; Brendel, J. C.; Larnaudie, S.; Barlow, T.; Jolliffe, K. A.; Perrier, S., Tunable Length of Cyclic Peptide–Polymer Conjugate Self-Assemblies in Water. *ACS Macro Letters* **2016,** *5* (10), 1119-1123.
(69) http://www.isis.stfc.ac.uk.
(70) Heenan, R. K.; Rogers, S. E.; Turner, D.; Terry, A. E.; Treadgold, J.; King, S. M., Small Angle Neutron Scattering Using Sans2d. *Neutron News* **2011,** *22* (2), 19-21.
(71) http://www.mantidproject.org.
(72) Wignall, G. D.; Bates, F. S., Absolute calibration of small angle neutron scattering data. *J. Appl. Crystallogr.* **1987,** *20*, 28-40.
(73) Zemb, T.; Lindner, P., *Neutrons, X-rays and light: scattering methods applied to soft condensed matter*. North-Holland: 2002.
(74) Bressler, I.; Kohlbrecher, J.; Thunemann, A. F., SASfit: a tool for small-angle scattering data analysis using a library of analytical expressions. *Journal of Applied Crystallography* **2015,** *48* (5), 1587-1598.
(75) Ulbrich, K.; Šubr, V.; Strohalm, J.; Plocová, D.; Jelínková, M.; Říhová, B., Polymeric drugs based on conjugates of synthetic and natural macromolecules: I. Synthesis and physico-chemical characterisation. *J. Controlled Release* **2000,** *64* (1), 63-79.
(76) Boyd, B. J.; Kaminskas, L. M.; Karellas, P.; Krippner, G.; Lessene, R.; Porter, C. J. H., Cationic Poly-l-lysine Dendrimers: Pharmacokinetics, Biodistribution, and Evidence for Metabolism and Bioresorption after Intravenous Administration to Rats. *Mol. Pharmaceutics* **2006,** *3* (5), 614-627.
(77) Zhang, Y.; Huo, M.; Zhou, J.; Xie, S., PKSolver: An add-in program for pharmacokinetic and pharmacodynamic data analysis in Microsoft Excel. *Computer Methods and Programs in Biomedicine 99* (3), 306-314.